Electronic Supplementary Material (ESI) for Chemical Communications.
This journal is © The Royal Society of Chemistry 2017

Supporting Information

Electrochemical Cycling and Beyond: Unrevealed Activation of MoO_3 for Electrochemical Hydrogen Evolution Reactions

Pitchai Thangasamy[a,b], Nagarajan Ilayaraja[a], Duraisamy Jeyakumar*[a] and Marappan Sathish [a,b]

[a]Functional Materials Division, [b]Academy of Scientific and Innovative Research (AcSIR), CSIR-Central Electrochemical Research Institute, Karaikudi-630 003, Tamil Nadu, India.
E. mail: marappan.sathish@gmail.com; msathish@cecri.res.in
duraisamyjeyakumar@gmail.com

Experimental section:

Synthesis of α-MoO_3 nanorods:

In a typical synthesis, 0.617 g (0.5 mmol) of ammonium heptamolybdate tetrahydrate was dissolved in 25 mL water and 1 mL of nitric acid was added into the solution followed by the addition of sodium dodecyl sulfate (SDS). The final solution was stirred well for 30 min and transferred into stainless steel reactor vessel (35 mL capacity) and sealed. The sealed reactor was then placed in a pre-heated (400° C) vertical tubular furnace for 30 min. At the tenure of the reaction, the sealed reactor was quenched in an ice cold water bath. MoO_3 was also prepared using hydrothermal route using the same recipe in 50 mL Teflon-lined stainless steel autoclave at 180°C for 24 h. The resultant products were collected and washed with water and ethanol. The light yellow colour product of α-MoO_3 was dried at 60 °C for 6 h in a vacuum oven. The MoO_3 powder obtained by SCF and hydrothermal method was denoted as S-MoO_3 and H-MoO_3, whereas the commercial powder (SRL, INDIA, 99.5%) is denoted as C-MoO_3. For the comparision purpose, thermally reduced S-MoO_3 product (T-S-MoO_3) was prepared by heating the S-MoO_3 sample at 500 °C for 2 h in hydrogen atmosphere.

Structural characterization of α-MoO_3 nanorods:

The powder XRD data were obtained using a PAN Analytical X' pert PRO Model X-ray Diffractometer with Cu K_α radiation (α = 1.5418 Å) from 10-80° at 0.02° step and a count time of 0.2s. The structural integrity of S-MoO_3 and H-MoO_3 was confirmed by FT-IR analysis from 400 to 4000 cm^{-1} using KBr pellet technique in TENSOR 27 spectrometer (Bruker). Raman spectra using laser Raman system (RENISHAW Invia laser Raman microscope) equipped with a semiconducting laser with a wavelength of 633 nm. The surface morphology and transparent nature of α-MoO_3 were identified using scanning electron microscopy (SEM) (Hitachi S-3000H, Japan) with an accelerating voltage of 0.3–30 kV. Transmission Electron Microscopy (TEM) and High Resolution Transmission Electron Microscopy (HR-TEM) images were taken by Tecnai G^2 20 and Tecnai G^2 F20 S-Twin working at an accelerating voltage of 200 kV, respectively. The reduction of α-MoO_3 was revealed by X-ray photoelectron spectroscopy (XPS) analysis using Thermo Scientific MULTILAB 2000 base system with X-ray, Auger and ISS attachments containing Twin Anode Mg/Al (300/400 W) X-ray source.

Electrochemical characterization:

All electrochemical studies were carried out using Autolab potentiostat-galvanostat (model PGSTAT-30) electrochemical workstation in a standard three–electrode setup in 0.5 M H_2SO_4 electrolyte solution. The as-synthesized transparent α-MoO_3 nanorods were used to modify a GC electrode surface by drop-casting method. A catalytic ink was formulated as follows. A mixture of 2.0 mg of α-MoO_3 catalyst and 50 µL Nafion solution was dispersed in 250 µL of water and sonicated for 30 min to form a homogeneous ink. 5.0 µL of α-MoO_3 catalyst ink was drop casted on GC electrode surface and air dried for few hours, and was used as working electrode. For the CV measurements, Pt wire and saturated calomel electrode (SCE) were used as counter electrode and reference electrode, respectively. There was no gas purging before or during the electrochemical measurements. The potential of the SCE reference electrode was calibrated to a reversible hydrogen electrode (RHE). The conversion of α-MoO_3 into monoclinic MoO_2 and MoO_{3-x} was studied in the potential range from +0.35 to -0.55 V (*vs.* RHE) with a scan rate of 50 mV s^{-1}. The HER electrocatalytic activity was examined using CV with a scan rate of 10 mV s^{-1} and 50 mV s^{-1} at room temperature.

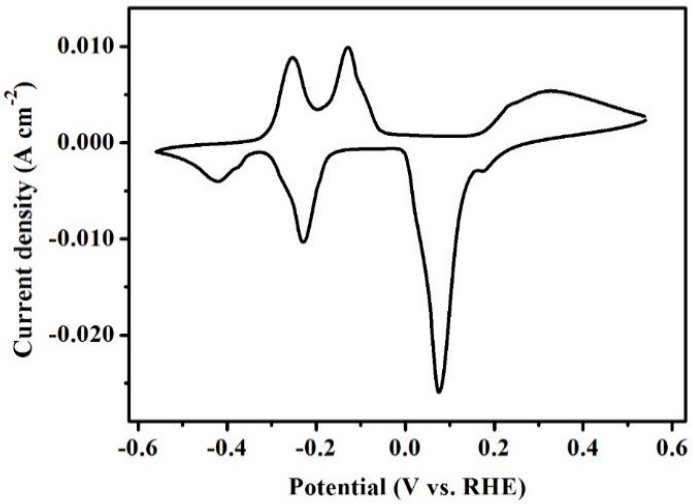

Fig. S1 Cyclic voltammogram of the S-MoO_3 on GC electrode in 0.5 M H_2SO_4 at a 10 mV s^{-1} scan rate.

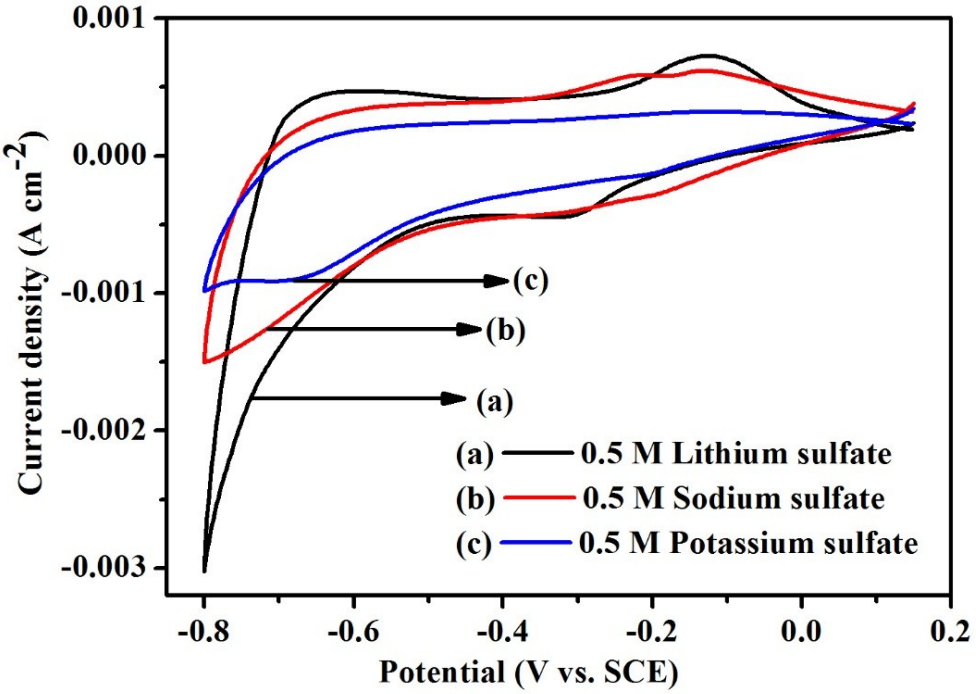

Fig. S2 Cyclic voltammogram of the S-MoO_3 on GC electrode in different electrolyte medium with a scan rate of 10 mV s^{-1}.

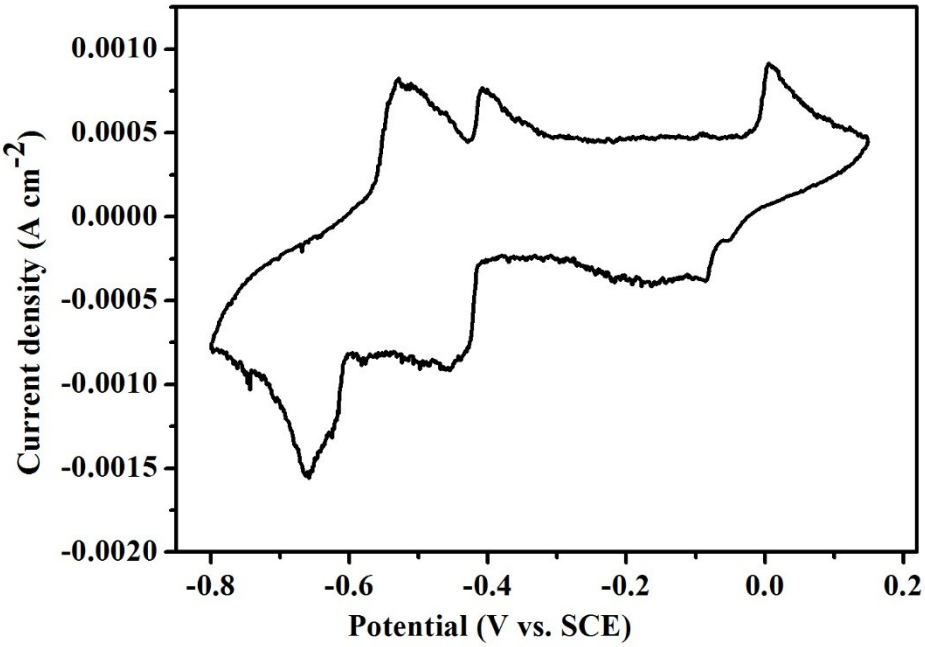

Fig. S3 Cyclic voltammogram of the C-MoO_3 on GC electrode in 0.5 M H_2SO_4 with a scan rate of 10 mV s^{-1}.

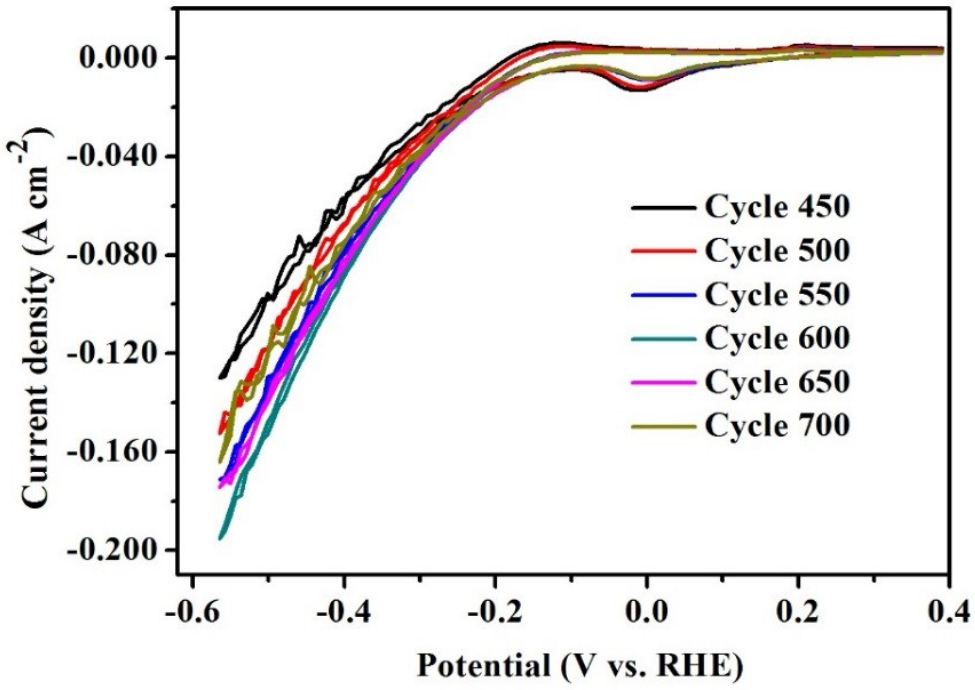

Fig. S4 Continuous cyclic voltammograms (after 400 cycles) of the S-MoO_3 at 50 mV s^{-1} scan rate.

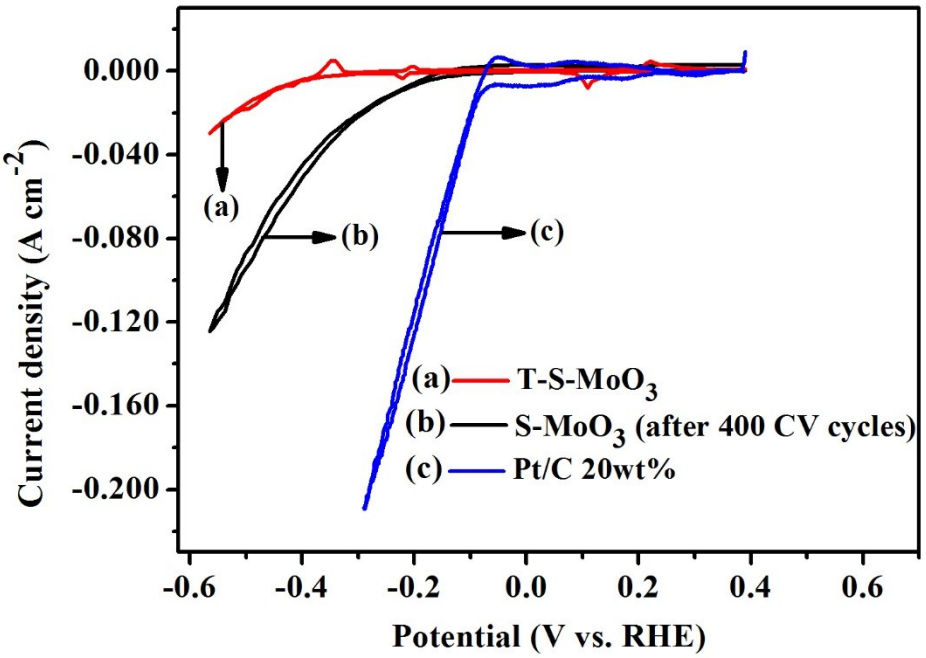

Fig. S5 Cyclic voltammograms of (a) T-S-MoO_3, (b) S-MoO_3 after 400 cycles and (c) commercial Pt/C 20wt% at 50 mV s^{-1} scan rate.

Electrochemical studies of S-MoO_3 in nitrogen and oxygen saturated electrolyte:

To understand the effect/reduction of dissolved oxygen on HER, nitrogen-saturated and oxygen-saturated electrolyte solutions were used for the electrochemical studies. It was noticed that a significant decrease in redox peak currents with slight shift in the peak positions for S-MoO_3 in nitrogen purged electrolyte compared to nitrogen unpurged electrolyte (Fig. S6a). It indicated that insertion and deinsertion of hydrogen ions in α-MoO_3 thin films on GC electrode surface was limited since molecular nitrogen occupies in the active sites and interlayers of α-MoO_3 where insertion/deinsertion process could take place by a hydrogen ion. However, electrochemical cycling induced reduction behaviour was also observed for S-MoO_3 sample in nitrogen saturated electrolyte (Fig. 6b). It is worthy to note that electrochemical reduction and the corresponding HER of S-MoO_3 are more substantial in nitrogen unpurged electrolyte (Fig. 6c). This may be due to the contribution of oxygen reduction reaction over HER. Further, CV of S-MoO_3 sample was recorded before and after O_2 gas purging (Fig. 6d). It can be clearly seen that there is no significant changes in the peak position and peak current except the first reduction peak in the oxygen saturated electrolyte. It implies that presence of excess dissolved oxygen in the electrolyte system doesn't has any role over the electrochemical reduction process.

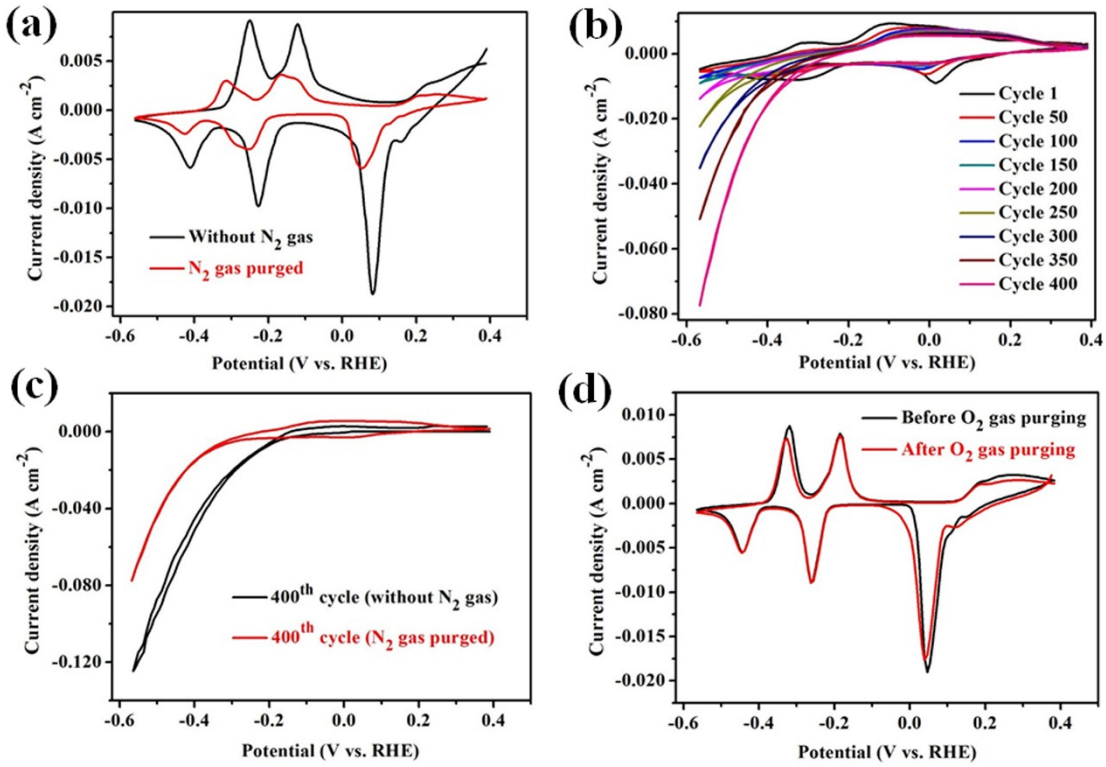

Fig. S6 (a) Cyclic voltammogram of the S-MoO_3 in nitrogen purged and unpurged 0.5 M H_2SO_4 electrolyte with a scan rate of 10 mV s^{-1}, (b) Continuous cyclic voltammograms (400 cycles) of the S-MoO_3 in nitrogen purged 0.5 M H_2SO_4 electrolyte at 50 mV s^{-1} scan rate, (c) Comparision of cyclic voltammogram for S-MoO_3 in nitrogen purged and unpurged 0.5 M H_2SO_4 electrolyte after 400 cycles with a scan rate of 50 mV s^{-1} and (d) Cyclic voltammogram of the S-MoO_3 in oxygen purged and unpurged 0.5 M H_2SO_4 electrolyte with a scan rate of 10 mV s^{-1}.

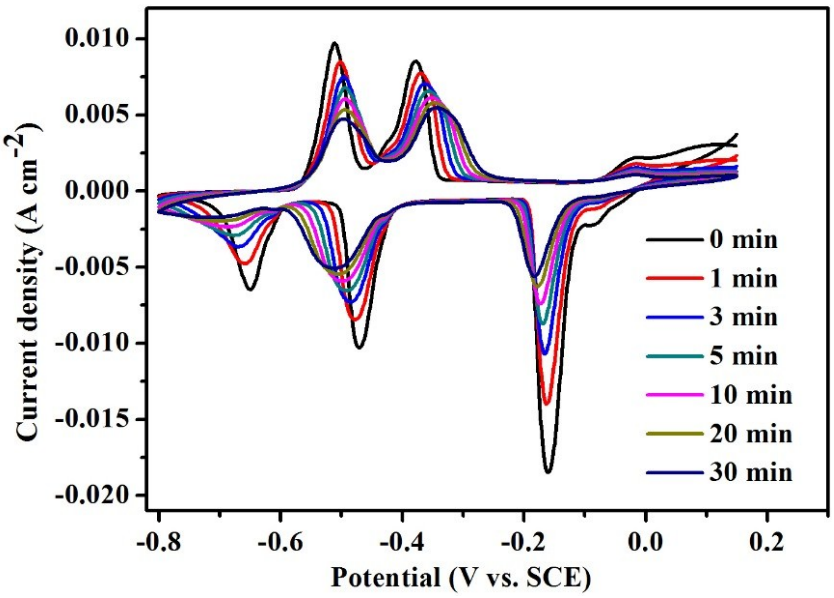

Fig. S7 Cyclic voltammograms of the S-MoO_3 in 0.5 M H_2SO_4 with a scan rate of 10 mV s^{-1} at different holding times.

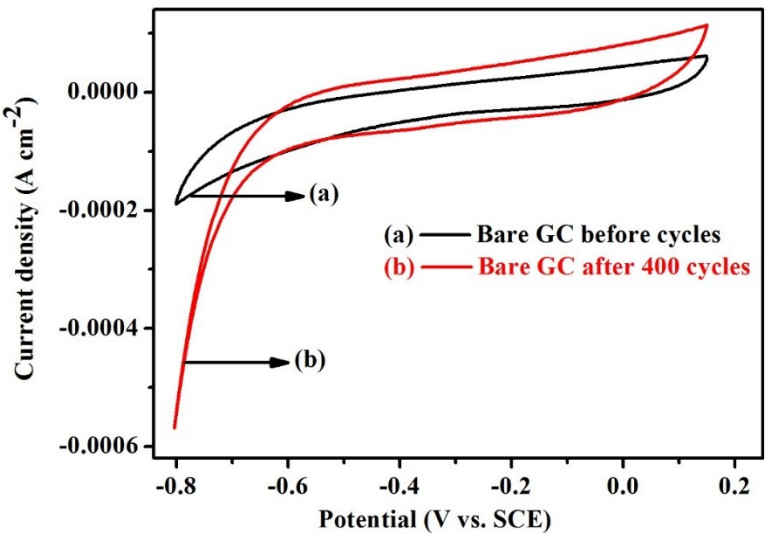

Fig. S8 Cyclic voltammograms of (a) before and (b) after 400 cycles of the bare GC electrode in 0.5 M H_2SO_4 with a scan rate of 50 mV s^{-1}.

XRD, FT-IR and Raman spectra:

Fig. S9A shows the XRD pattern of S-MoO_3, H-MoO_3 and C-MoO_3 (before the electrochemical cycling), it can be readily indexed to α-MoO_3 phase (JCPDS card No: 00-005-0508) with lattice constants of a = 3.962, b = 13.858 and c = 3.697 Å. There are no additional peaks in the XRD pattern clearly indicating the product is highly phase pure and free from metastable phases like hexagonal and monoclinic phases. The intensity of sharp diffraction peaks observed for the S-MoO_3 and C-MoO_3 are much higher compared to H-MoO_3. It is worthy to note here that S-MoO_3 prepared in a short reaction time results the formation of crystalline α-MoO_3 without any further high temperature post annealing. The XRD pattern of T-S-MoO_3 and S-MoO_3 after 400 cycling was recorded and presented in Fig. S9B. The XRD pattern of S-MoO_3 after 400 cycles shows two major diffraction peaks at 13.12 and 26.06°, and a very weak peak at 39.39°, the peak at 26.06° was well matched with the monoclinic MoO_2 pattern (JCPDS card No: 01-076-1807). The peaks at 13.12° and 39.39° are attributed to the reduced MoO_{3-x}. This may be attributed due to the more oxygen vacancies created in MoO_3 and/or particle size reduction and strain. The observations suggest there is conversion of MoO_3 to monoclinic MoO_2 and MoO_{3-x} as is further confirmed from XPS and HR-TEM analysis of these samples. The thermal reduction of S-MoO_3 results the formation of monoclinic MoO_2. Both H-MoO_3 and C-MoO_3

samples also showed diffraction lines corresponding to monoclinic MoO_2/MoO_{3-x} after 400 cycles (Fig. S10).

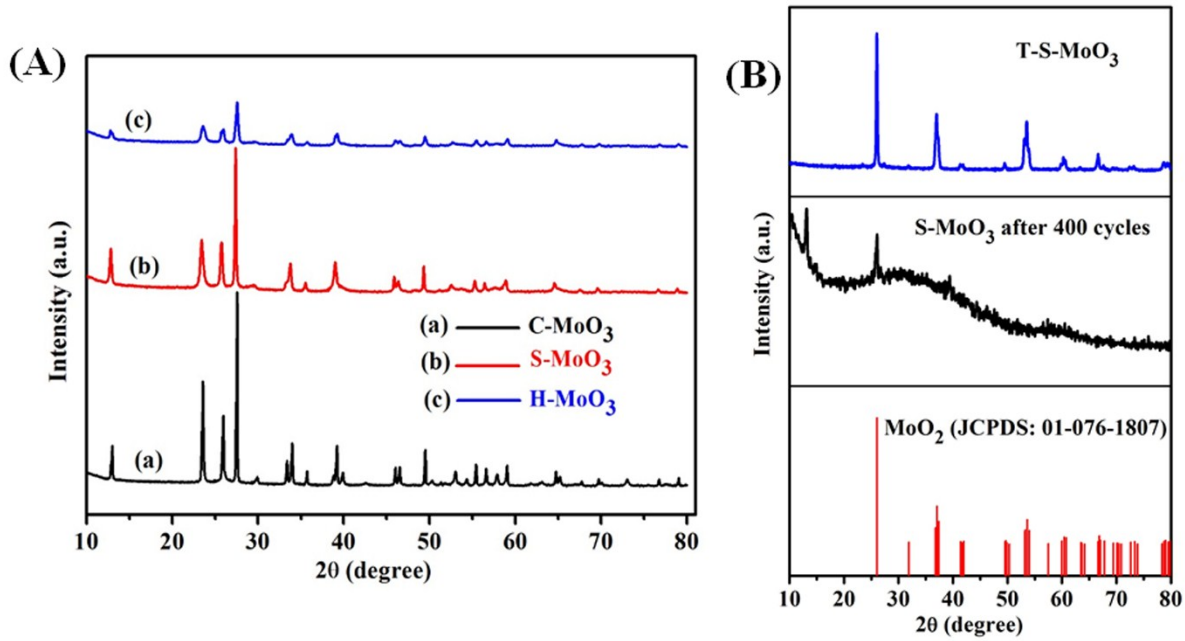

Fig. S9 XRD patterns of (A) MoO_3 powders: (a) C-MoO_3, (b) S-MoO_3 and (c) H-MoO_3 and (B) T-S-MoO_3, S-MoO_3 after 400 cycles and the standard JCPDS card for monoclinic MoO_2.

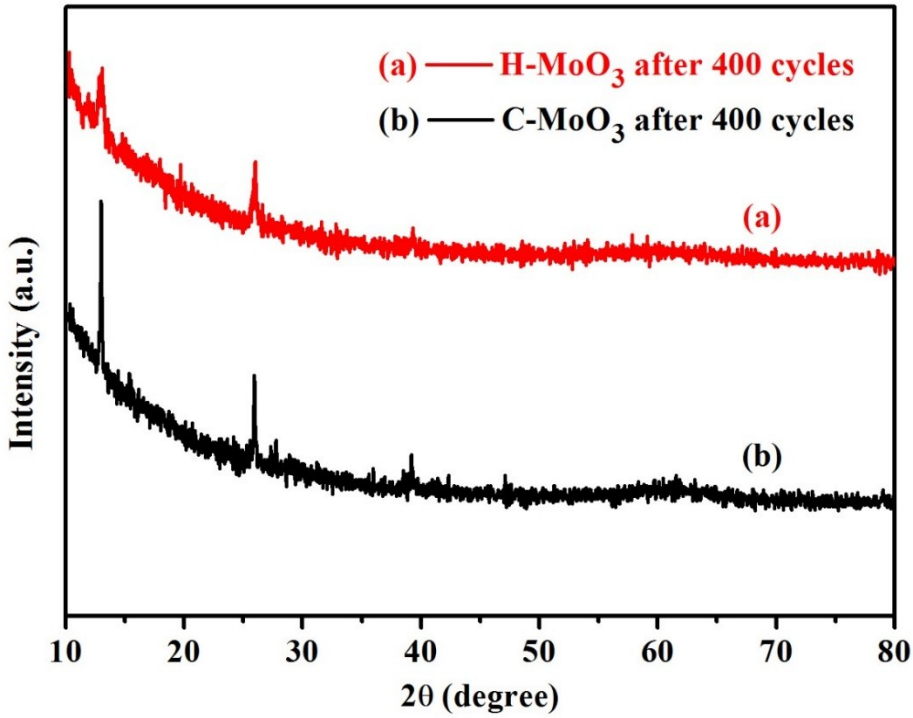

Fig. S10 XRD patterns of (a) H-MoO_3 and (b) C-MoO_3 after 400 cycles.

The FT-IR spectra of S-MoO_3, H-MoO_3 and C-MoO_3 confirms the existence of various Mo-O bands (Fig. S11). The band at 997 cm^{-1} is attributed to the stretching vibrations of the terminal Mo = O bond, which is an indicator of the layered orthorhombic MoO_3 phase.[S1] The distinct bands observed at 849 and 555 cm^{-1} are ascribed to the vibrations of Mo^{6+} ions in Mo-O-Mo units and the bending vibration of oxygen atoms linked to three molybdenum atoms, respectively. These bands are typical characteristics of crystalline α-MoO_3 phase among other metastable phases of MoO_3.[S2] While, there are three characteristic bands at 995, 822 and 666 cm^{-1} was observed in Raman spectra (Fig. S12). The observed Raman lines are in good agreement with previously reported α-MoO_3.[S3,S4] The peaks at 995 and 822 cm^{-1} can be attributed to the vibration of asymmetric terminal oxygen and doubly coordinated bridging oxygen (Mo-O-Mo), respectively. While the band at 666 cm^{-1} is due to the stretching vibration of triply coordinated oxygen.[S2] In addition, characteristic peaks that correspond to the various bending modes of α-MoO_3 could be seen between 200 and 400 cm^{-1}.

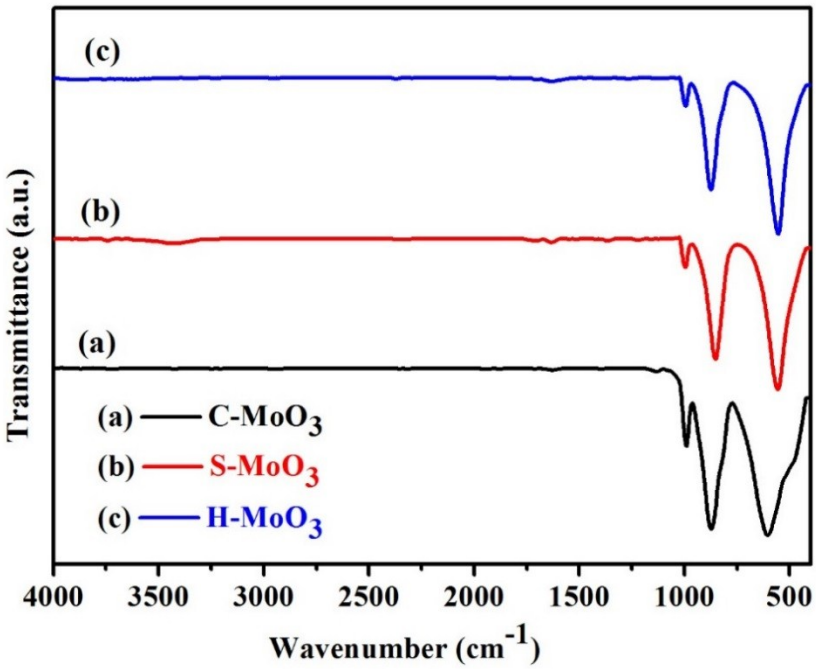

Fig. S11 FT-IR spectra of MoO_3 powders: (a) C-MoO_3, (b) S-MoO_3 and (c) H-MoO_3.

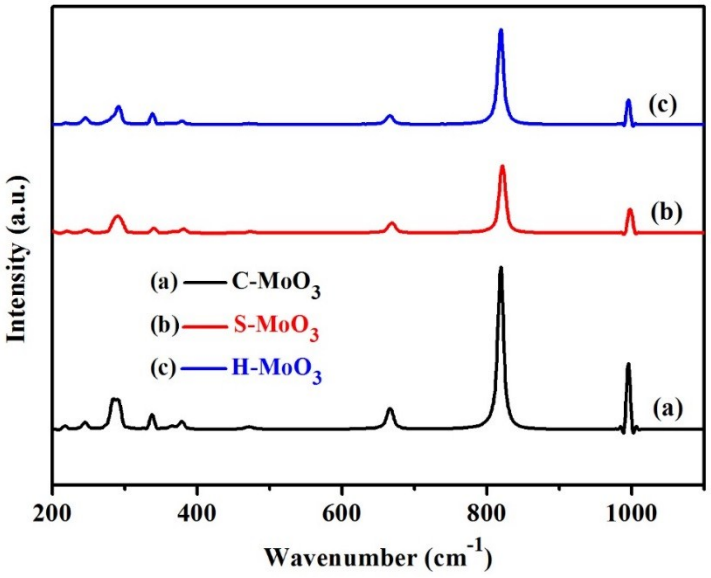

Fig. S12 Raman spectrum of (a) C-MoO_3, (b) S-MoO_3 and (c) H-MoO_3.

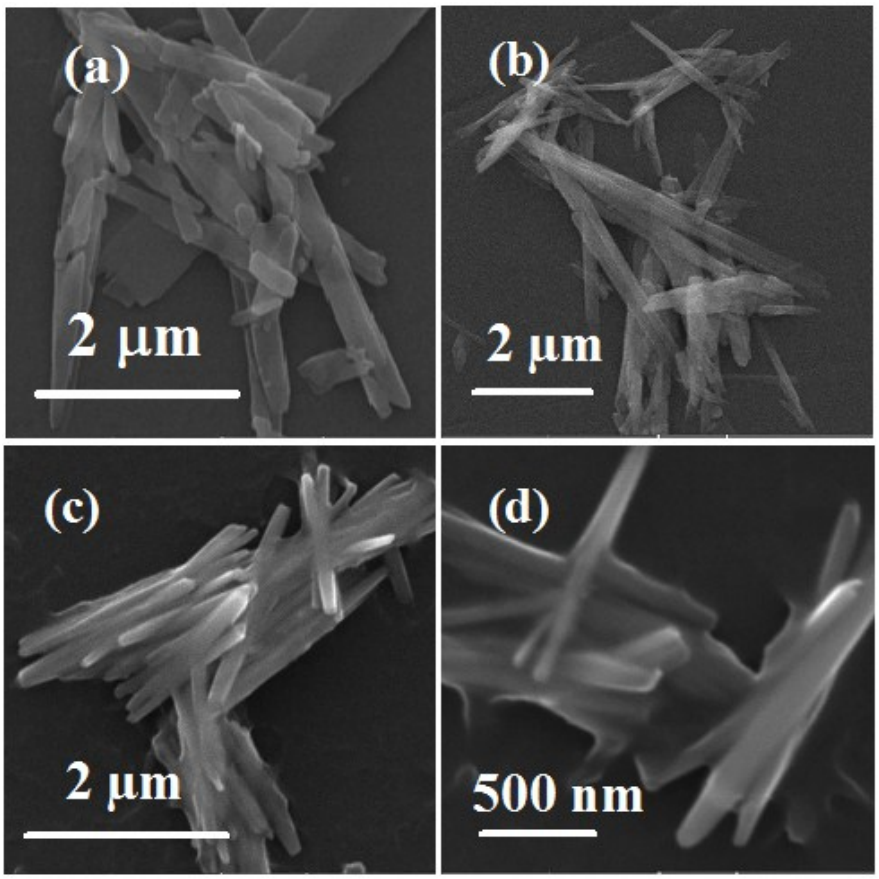

Fig. S13 SEM images of (a&b) S-MoO_3 before and (c&d) after 400 cycles.

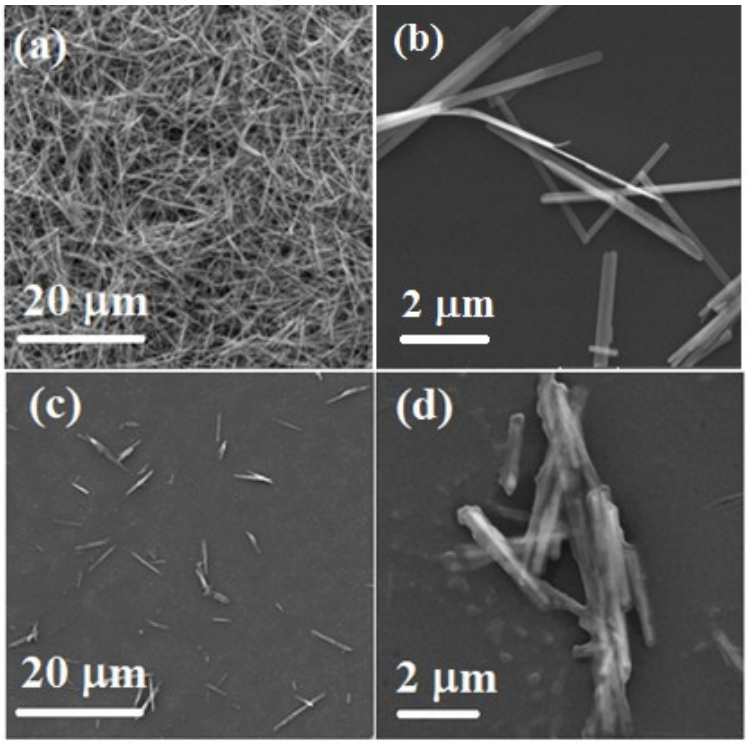

Fig. S14 SEM images of (a&b) H-MoO_3 before and (c&d) after 400 cycles.

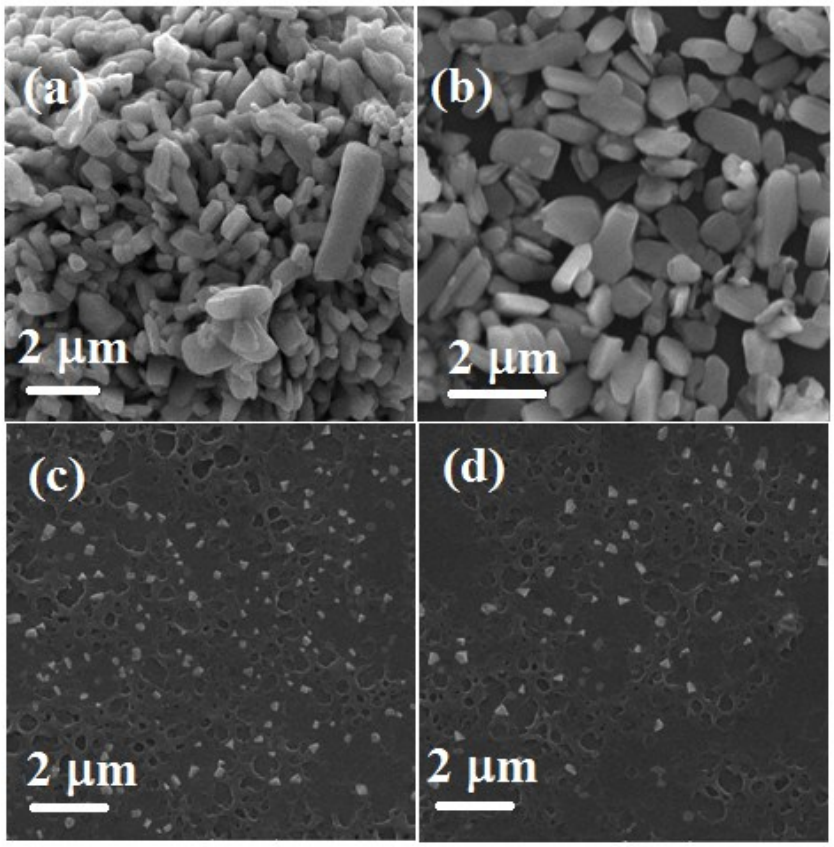

Fig. S15 SEM images of (a&b) C-MoO_3 before and (c&d) after 400 cycles.

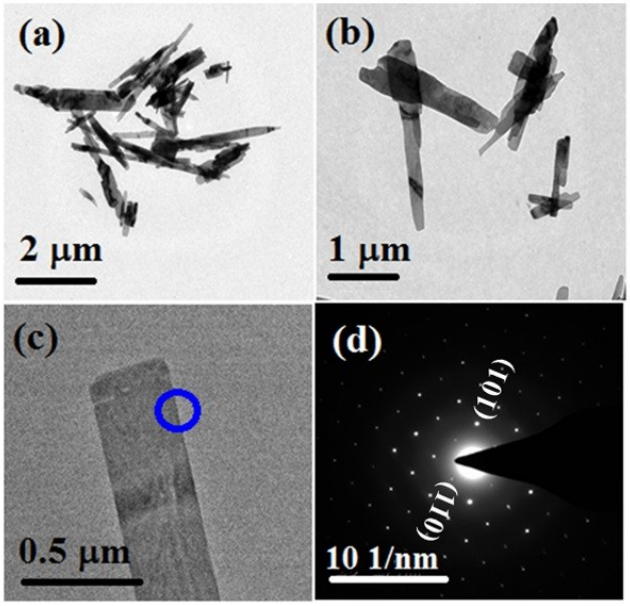

Fig. S16 TEM images of (a-c) S-MoO_3 and (d) the corresponding SAED pattern of nanorods.

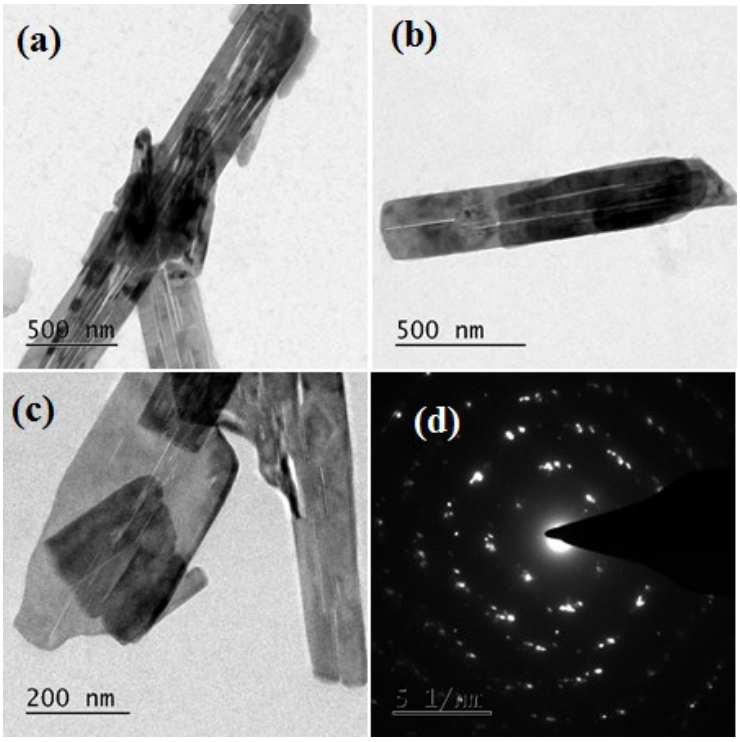

Fig. S17 TEM images (a-c) for after 400 cycles of S-MoO_3 and (d) the corresponding SAED pattern.

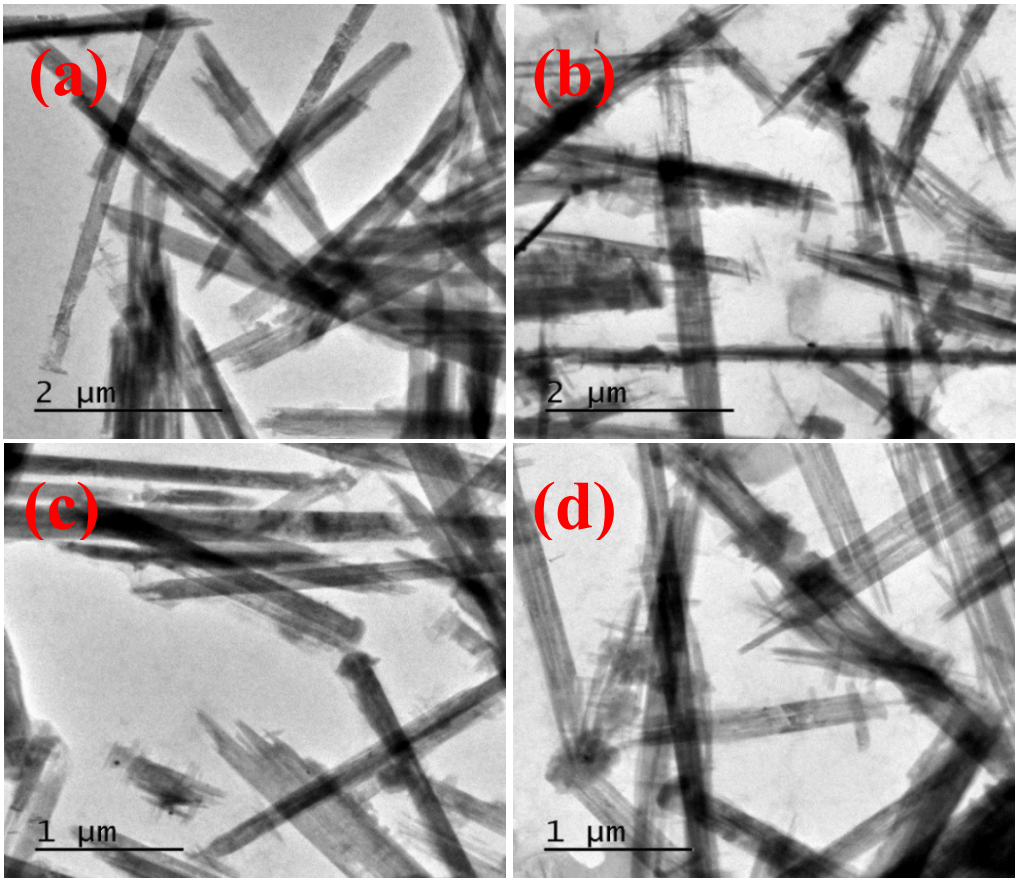

Fig. S18 TEM images of (a-d) H-MoO_3 after 400 cycles.

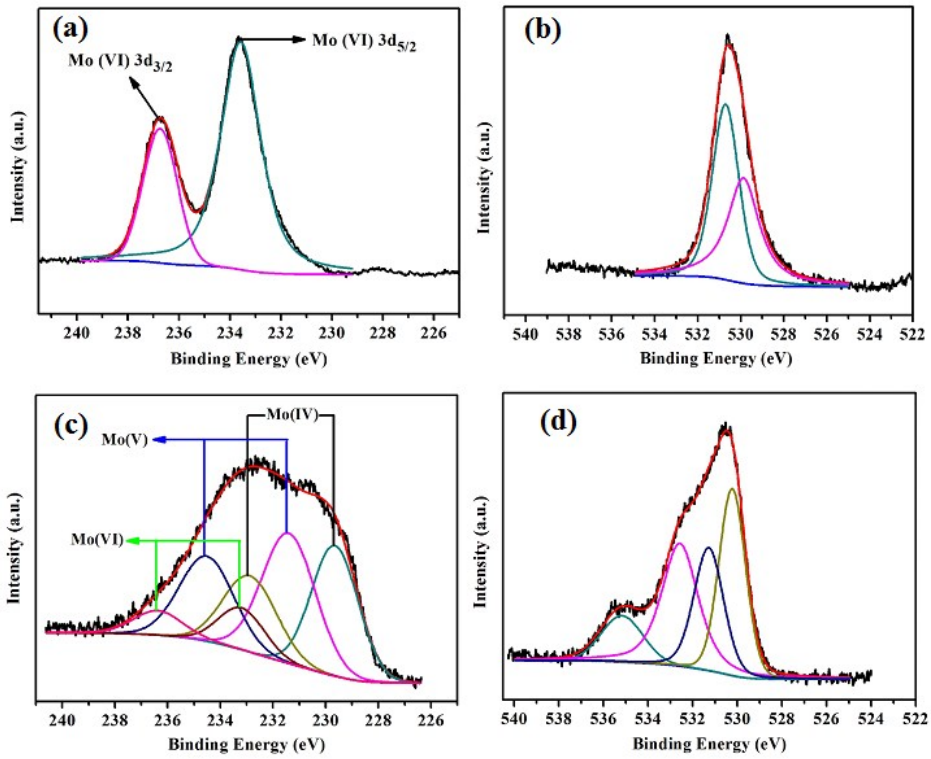

Fig. S19 XPS spectra: (a)&(b) and (c)&(d) Mo3d and O1s spectra of before and after 400 cycles of the S-MoO_3, respectively.

References:

S1 S. Morandi, G. Ghiotti, A. Chiorino and E. Comini, *Thin Solid Films,* 2005, **490**, 74.

S2 Y. Chen, C. Lu, L. Xu, Y. Ma, W. Hou and J.-J. Zhu, *CrystEngComm.,* 2010, **12**, 3740.

S3 T. Siciliano, A. Tepore, E. Filippo, G. Micocci and M. Tepore, *Mater. Chem. Phys*., 2009, **114**, 687.

S4 K. K. Zadeh, J. Tang, M. Wang, K. L. Wang, A. Shailos, K. Galatsis, R. Kojima, V. Strong, A. Lech, W. Wlodarski and R. B. Kaner, *Nanoscale,* 2010, **2**, 429.